This article has been accepted for publication in a future issue of this journal, but has not been fully edited. Content may change prior to final publication. Citation information: DOI 10.1109/TPWRD.2016.2545923, IEEE Transactions on Power Delivery

Fault Detection and Faulted Line Identification in Active Distribution Networks using Synchrophasors-based Real-Time State Estimation

Marco Pignati*, *Member, IEEE,* Lorenzo Zanni*, *Member, IEEE,* Paolo Romano, *Member, IEEE,* Rachid Cherkaoui, *Senior Member, IEEE,* Mario Paolone, *Senior Member, IEEE*

***Abstract*—We intend to prove that PMU-based state estimation processes for active distribution networks exhibit unique time determinism and refresh rate that make them suitable to satisfy the time-critical requirements of protections as well as the accuracy requirements dictated by faulted line identification. In this respect, we propose a real-time fault detection and faulted line identification functionality obtained by computing parallel synchrophasor-based state estimators. Each state estimator is characterized by a different and augmented topology in order to include a floating fault bus. The selection of the state estimator providing the correct solution is done by a metric that computes the sum of the weighted measurement residuals. The proposed process scheme is validated by means of a real-time simulation platform in which an existing active distribution network is simulated together with a PMU-based monitoring system. The proposed process is shown to be suitable for active and passive networks, with solid-earthed and unearthed neutral, for low and high impedance faults of any kind (symmetric and asymmetric) occurring at different locations.**

***Index Terms*—Active distribution networks, protection, fault detection, fault location, phasor measurement units, real-time state estimation, real-time simulation.**

I. Introduction

THE massive integration of distributed generation (DG) is leading to important changes in the operation of distribution networks. In this context, the protection schemes are experiencing major transformations (e.g., [1]). Traditionally, fault detection together with the associated relaying schemes and fault location[1] functionalities have been considered as separate processes since the latter usually requires computational efforts that do not fit the time latencies needed by the protections. Along the years, several fault detection and location methods have been proposed for distribution networks. The majority of them are based on impedance measurements (e.g., [2]), travelling waves (e.g., [3]) or phasor measurements (e.g., [4]). However, to the best of the authors' knowledge, the existing literature has marginally discussed the possibility of merging the detection and location functionalities. The recent literature has also discussed the use of phasor measurement units (PMUs) to develop low-latency and high-refresh rate real-time state estimators (SEs) for distribution networks [5]–[7]. The use of low-cost hardware platforms is contributing to the massive use of PMUs in distribution networks [8]. Dedicated installations in real distribution networks have already demonstrated the feasibility of this solution [9], [10]. As an example, the active distribution network (ADN) in [9] is equipped with PMUs in every bus measuring nodal voltages and injected current synchrophasors. By leveraging the distribution network operator need for real-time monitoring, other applications, such as fault detection and location, might be developed using this same metering infrastructure (e.g., [11], [12]).

Within the context of PMU-based protections, this work discusses the possibility of merging the relaying and fault location functionalities for active distribution networks by using PMU-based real-time state estimation. Indeed, beside their capability of bad data filtering, real-time SEs are characterized by high rejection of measurement noise [13] and low time latency [9]. The former property improves the assessment of the fault position, whilst the latter supports the stringent time requirements of protections.

The number of papers available in the current literature that are exploring the possibility of localizing faults by means of PMU-based state estimation is limited to [11] and [14]. In [11] the fault is detected by using bad data identification techniques. An augmented state vector and the corresponding Jacobian matrix are then produced to estimate the fault location. In [14], the fault is detected by analyzing the residual vector of a synchrophasor estimator in order to have a backup protection scheme.

The method proposed in this paper differs from the existing ones since it relies on a PMU-only based sensing infrastructure to identify, in real-time, the line affected by the fault, the fault type and the current drained by the fault. The proposed method does not change regardless to the type of network, the type of fault, the fault impedance or the presence of DG. This flexibility enables the use of the proposed approach as a single protection scheme in active distribution networks. The line affected by the fault is determined by comparing the outputs of several parallel SEs using the weighted measurement residuals (WMRs). The validation is carried out for different noise levels derived from PMU measurements recorded in a real distribution network. Furthermore, the paper contains the validation performed on a real-time simulator, where a real

*The first two Authors equally contributed to this manuscript.

The Authors are with the École Polytechnique Fédérale de Lausanne EPFL, CH-1015, Lausanne, Switzerland.

The research leading to these results has received funding from the European Community's Seventh Framework Programme FP7-ICT-2011-8 under grant agreement n° 318708 (C-DAX) and also from the NanoTera Swiss National Science Foundation project S3-Grids. The Authors alone are responsible for the content of this paper.

[1]Henceforth in the paper, the term faulted line identification is used interchangeably with the term fault location.

This article has been accepted for publication in a future issue of this journal, but has not been fully edited. Content may change prior to final publication. Citation information: DOI 10.1109/TPWRD.2016.2545923, IEEE Transactions on Power Delivery

network model and PMUs are implemented. To be noted that the PMU synchrophasor extraction algorithm used to estimate the synchrophasor measurements is the same as the one used in the context of a real PMU-monitored active distribution network [9]. All these elements are setting realistic operating conditions for the validation of the proposed method. Finally, an analysis of the latencies introduced by different elements in the fault identification chain is provided.

This paper is structured as follows: Section II provides the background on the state estimation theory and describes the proposed faulted line identification method. Section III illustrates the simulation environment with particular focus on the measurement noise model. Section IV provides the performance assessment of the method with respect to the considered scenarios. Finally, Section V summarizes the results of the paper.

II. The proposed method

We suppose to observe the state of an ADN by measuring nodal voltages and injected current synchrophasors in d network buses. This assumption enables the use of linear SEs, as explained later in this section. In what follows, we summarize the analytical formulation of a linear weighted least squares state estimator (LWLS-SE) for the case of a generic three-phase (3-ph) network.

A. Linear weighted least squares state estimator

The state of a 3-ph network with n buses $\mathbf{x} \in \mathbb{R}^N$ ($N = 3n \cdot 2$) can be expressed in rectangular coordinates as follows:

$$\mathbf{x} = [\mathbf{V}_{1_{re}}^{a,b,c}, ..., \mathbf{V}_{n_{re}}^{a,b,c}, \mathbf{V}_{1_{im}}^{a,b,c}, ..., \mathbf{V}_{n_{im}}^{a,b,c}]^T \tag{1}$$

where

$$\begin{aligned} \mathbf{V}_{i_{re}}^{a,b,c} &= [V_{i_{re}}^a, V_{i_{re}}^b, V_{i_{re}}^c] \\ \mathbf{V}_{i_{im}}^{a,b,c} &= [V_{i_{im}}^a, V_{i_{im}}^b, V_{i_{im}}^c] \end{aligned} \tag{2}$$

are respectively the 3-ph real and imaginary parts of the voltage phasors at bus #i.

We assume to have PMUs installed in d network buses that measure nodal voltages and injected current synchrophasors. The set of network buses equipped with PMUs is $\mathscr{D}$. Therefore, the measurement set $\mathbf{z} \in \mathbb{R}^D$ ($D = 3d \cdot 4$) is composed of the real and imaginary parts of $3d$ phase-to-ground voltage phasors and $3d$ injected current phasors. It is defined as:

$$\mathbf{z} = [\mathbf{z}_V, \mathbf{z}_I]^T \tag{3}$$

where

$$\begin{aligned} \mathbf{z}_V &= [..., \mathbf{V}_{i_{re}}^{a,b,c}, ..., \mathbf{V}_{i_{im}}^{a,b,c}, ...]^T \\ \mathbf{z}_V &= [..., \mathbf{I}_{i_{re}}^{a,b,c}, ..., \mathbf{I}_{i_{im}}^{a,b,c}, ...]^T \end{aligned} \tag{4}$$

in which $i \in \mathscr{D}$.

The equation that relates the measurements with the state variables is:

$$\mathbf{z} = \mathbf{H}\mathbf{x} + \mathbf{v} \tag{5}$$

where $\mathbf{H}$ is the measurement matrix and $\mathbf{v}$ is the measurement noise vector. We assume that $\mathbf{v}$ is a Gaussian white noise:

$$p(\mathbf{v}) \sim \mathcal{N}(0, \mathbf{R}) \tag{6}$$

where $\mathbf{R}$ is the measurement noise covariance matrix that represents the accuracy of the measurement devices. Since we assume the measurement errors are not correlated, it is defined as:

$$\mathbf{R} = diag(\sigma_1^2, ..., \sigma_D^2). \tag{7}$$

It is worth observing that the accuracies of the synchrophasors are expressed in polar coordinates. Since we here adopt rectangular coordinates, we need to project them from polar to rectangular. In this projection, the normality of the error distributions in rectangular coordinates is granted if and only if the deviations in amplitude and phase are small, which is the case for PMUs.

The measurement matrix $\mathbf{H}$ is composed of two sub-matrices $\mathbf{H}_V$ and $\mathbf{H}_I$:

$$\mathbf{H} = \begin{bmatrix} \mathbf{H}_V \\ \mathbf{H}_I \end{bmatrix}. \tag{8}$$

$\mathbf{H}_V$ relates the voltage measurements to the state and consists of ones and zeros that are directly inferred from (5). $\mathbf{H}_I$ relates the injected current measurements to the state and contains the elements of the network admittance matrix. The real and imaginary parts of the 3-ph injected current phasors are:

$$I_{i_{re}}^p = \sum_{h=1}^{n} \sum_{l=1}^{3} [G_{ih}^{pl} V_{h_{re}}^l - B_{ih}^{pl} V_{h_{im}}^l] \tag{9}$$

$$I_{i_{im}}^p = \sum_{h=1}^{n} \sum_{l=1}^{3} [B_{ih}^{pl} V_{h_{re}}^l + G_{ih}^{pl} V_{h_{im}}^l] \tag{10}$$

where i and h are the bus indexes, p and l are the phase indexes, G and B are respectively the real and imaginary parts of the elements of the network admittance matrix. Therefore, $\mathbf{H}_I$ is derived from (9) and (10) as:

$$\mathbf{H}_I = \begin{bmatrix} G_{ih}^{pl} & -B_{ih}^{pl} \\ B_{ih}^{pl} & G_{ih}^{pl} \end{bmatrix}. \tag{11}$$

Note that the formulation of the problem in rectangular coordinates allows to define a measurement matrix $\mathbf{H}$ that does not contain any approximation. Indeed, since we assume that the network admittance matrix is not affected by errors, $\mathbf{H}$ is exact.

The LWLS-SE maximizes the likelihood that, as known, is equivalent to minimizing the following objective function:

$$J(\mathbf{x}) = \sum_{i=1}^{D} \frac{(z_i - \sum_{h=1}^{N} H_{ih} x_h)^2}{R_{ii}}. \tag{12}$$

Then we calculate the so-called *Gain matrix*:

$$\mathbf{G} = \mathbf{H}^T \mathbf{R}^{-1} \mathbf{H} \tag{13}$$

and the estimated state is equal to:

$$\widehat{\mathbf{x}}_{LWLS} = \mathbf{G}^{-1} \mathbf{H}^T \mathbf{R}^{-1} \mathbf{z}. \tag{14}$$

This article has been accepted for publication in a future issue of this journal, but has not been fully edited. Content may change prior to final publication. Citation information: DOI 10.1109/TPWRD.2016.2545923, IEEE Transactions on Power Delivery

B. Fault detection and location method

The proposed fault detection and location method relies on the following assumptions:

1) Knowledge of the network admittance matrix (i.e., $\mathbf{H}$ is exact). This assumption implies the knowledge of (i) network topology and (ii) line parameters. For (i), it has to be noted that PMUs are able to record and stream Boolean variables together with the synchrophasor data. These Boolean inputs may correspond, as it is the case for the real network described in this paper, to the status of the breakers connected to a given PMU-monitored substation. Once the status of all the breakers is collected by the phasor data concentrator, it is straightforward to obtain the incidence matrix of the network and, thus, its topology and the corresponding admittance matrix used in (11). This aspect is a further advantage of using PMUs for protection since the topology assessment can be easily reconstructed and time-tagged with limited latencies. In the case where not all the PMUs can measure the status of the breakers in the substation, the literature provides several methods to estimate the topology or detect topology errors, with or without using PMU measurements [15]–[18]. Concerning (ii), distribution networks are usually composed of overhead lines and cables that have a standard configuration with known electrical parameters. Therefore, we suppose that the network operator knows these characteristics.
2) The measurement noise covariance $\mathbf{R}$ is known. This is a common assumption in power systems since the characteristics of the measurement devices, and therefore their accuracy, is usually known in detail [5]–[7], [19], [20].
3) PMUs are installed in every bus: $D = N$. It is worth observing that the current literature has shown a growing interest in PMU deployment and their applications in distribution systems: recent publications have illustrated and discussed distribution networks equipped with PMUs in every bus [9], [21].
4) Due to the stringent time requirements of the targeted application, bad data are removed from the measurement set by using the pre-filtering algorithm described in [22] that was proved to be robust against faults.

Observation: A fault on a line can be modeled as an event that suddenly increases by one the total number of buses in the monitored network. This additional bus (hereafter called *virtual bus*) is between two real buses and absorbs the fault current.

Let consider a n-buses and m-lines ADN equipped with PMUs at every bus. We can define m parallel SEs fed with the same measurement set, but each one uses a slightly different network topology from the others. The difference in the topology is given by the position of the virtual bus. The j^{th} SE ($j = 1, ..., m$) considers the existence of a virtual bus in the middle of the j^{th} line by using an augmented state vector $\widetilde{\mathbf{x}}$. We add the virtual bus voltage phasors to the state defined in (1) as follows:

$$\widetilde{\mathbf{x}} = [V_{1_{re}}^{a,b,c}, ..., V_{n_{re}}^{a,b,c}, V_{n+1_{re}}^{a,b,c}, V_{1_{im}}^{a,b,c}, ..., V_{n_{im}}^{a,b,c}, V_{n+1_{im}}^{a,b,c}]^T \tag{15}$$

where $V_{n+1_{re}}^{a,b,c}$ and $V_{n+1_{im}}^{a,b,c}$ are respectively the real and imaginary parts of the voltage in the virtual bus. The measurement matrix $\mathbf{H}$ is modified accordingly for each SE.

During normal operating conditions, each of the m-virtual buses does not absorb any current and the different topologies do not play a role in the outputs of each SE. Therefore, the minimization of the objective function (12) will provide similar results for all the m-SEs so that:

$$\widetilde{\mathbf{x}}^j \backsimeq \mathbf{x}_{true} \quad \forall j \tag{16}$$

Let assume a generic fault (i.e., phase to ground, phase to phase or three phase) occurs in the line $L_{h,u}$ between buses #h and #u. From the physical point of view, a certain amount of current is drawn from an unknown position between buses #h and #u. The j^{th} SE uses the measurement set $\mathbf{z}$ and its own specific topology (namely its matrix $\mathbf{H}^j$) to compute the estimated state according to (13) and (14). Let assume that the f^{th} SE has the virtual bus placed in the middle of line $L_{h,u}$. Intuitively, its topology is the closest one to the real network, even if the fault is not located exactly in the middle of the line. Therefore, it provides an estimated state close to the true one:

$$\begin{aligned} &\widetilde{\mathbf{x}}^f \backsimeq \mathbf{x}_{true} \\ &\widetilde{\mathbf{x}}^j \neq \mathbf{x}_{true} \quad \forall j \neq f \end{aligned} \tag{17}$$

Since the position of the fault is not known a priori, it is necessary to identify the SE providing the best estimated state. The WMR is the metric used to determine the best SE:

$$WMR^j = \sum_{i=1}^{D} \frac{|\mathbf{z}_i - \widehat{\mathbf{z}}_i^j|}{\boldsymbol{\sigma}_{z_i}} \quad j \in [1, \ldots, m] \tag{18}$$

where $\widehat{\mathbf{z}}^j = \mathbf{H}^j \widehat{\mathbf{x}}^j$.

In case of no fault, the WMRs of all the SEs are very close to each other. By the time a fault occurs, $m-1$ SEs converge to a solution far from the true state and are characterized by high WMRs. The SE that has the virtual bus placed in the faulted line has the lowest WMR. Therefore, it is immediate to identify the line affected by the fault.

The detection of the fault is performed by comparing the mean of the WMRs of the m-SEs, called WMR_{mean}. When the difference between the WMR_{mean} of two consecutive time-steps has a sudden increase, a fault is detected (see Fig. 6 in Section IV-A). Moreover, the state returned by this SE is used, together with its admittance matrix, to compute the estimated fault currents. The phases of the virtual bus in which the estimated current differs from zero are the ones affected by the fault, so that also the fault type is identified.

A pseudo-algorithm that summarizes the proposed method is given in Fig. 1. For every new data set coming from the PMUs, we compute the WMRs of the parallel SEs and also their mean WMR_{mean}. Comparing the WMR_{mean} of two consecutive time-steps, we detect the presence of a fault. If a fault is detected, the index j of the SE associated to the minimum WMR identifies the faulted line. Finally, we can

This article has been accepted for publication in a future issue of this journal, but has not been fully edited. Content may change prior to final publication. Citation information: DOI 10.1109/TPWRD.2016.2545923, IEEE Transactions on Power Delivery

function IDENTIFY FAULT (LINE,CURRENT,TYPE)
  for each time-step k **do**
  compute $\text{WMR}_j \quad \forall j$
  if $\text{mean(WMRs)}\big|_k \gg \text{mean(WMRs)}\big|_{k-1}$ **then**
    $Fault \leftarrow 1$
    $j =$ index of min(WMRs)
    $Faulted\ Line \leftarrow j$
    $I^j = Y^j E^j$
    $Fault\ Current \leftarrow I^j_{virtual\ bus}$
    $Fault\ Type \leftarrow$ phases where $Fault\ current \neq 0$
  end if
  return $Faulted\ Line, Fault\ Current, Fault\ Type$
end function

Fig. 1. Pseudo-algorithm of the proposed fault detection and location method.

use the estimated state returned by the j^{th} SE to identify the fault type and estimate the fault current.

In summary, the proposed method allows to:

- detect the existence of a fault;
- identify the faulted line;
- identify the fault type (1-ph, 2-ph or 3-ph);
- estimate the fault current.

III. SIMULATION ENVIRONMENT

In order to assess the accuracy and time latency of the proposed method we have modeled both electrical network and measurement devices in a real-time simulator (RTS).

A. Network description

The considered network is a real 10-kV 3-ph distribution network located in the Netherlands and operated by Alliander. The network is being equipped with PMUs within the context of the EU project C-DAX [23]. It has 18 buses and its layout is reported in Fig. 2. The powers absorbed by the loads are unbalanced. The network is composed of underground cables with cross sections from 95 to 240 mm^2. Their electrical parameters are provided in the Appendix. The network has been modeled in SimPowerSystem™ and the simulations are run by using the Opal-RT RTS. The lines are modeled with the equivalent PI circuit, the upstream grid has a short-circuit power of 1000 MVA and it is modeled with the short-circuit impedance Z_{sc} (we assumed a resistance to reactance ratio $R_{sc}/X_{sc} = 1/10$). The high to medium voltage transformer can be either Yg-Yg or Yg-Y, according to the simulation scenario that might request earthed or unearthed neutral networks, respectively. The loads are modeled as star connections of impedances. In normal operating conditions they absorb approximately 1/4 of the rated power of the real transformers to which they are connected. Loads are connected to all the buses, from bus #2 to #18.

B. Description of the adopted PMUs

The modeled network has been equipped with PMUs in every bus measuring nodal voltage and injected current phasors. The PMU is based on the process illustrated in [8] that adopts the enhanced interpolated DFT algorithm to extract the synchrophasors. The implementation of this PMU into the RTS is described in [24]. The use of simulated PMUs makes the validation of the proposed method more realistic compared to the common practice of using synchrophasors generated from the true state. Indeed, the adoption of a real synchrophasor estimation algorithm allows to model the PMU's behavior during transients, i.e. its response time. The latter is mainly affected by the window length used by the algorithm and the position of the timestamp within the window. A comparison of the time evolution of the current phasor magnitude estimated by the modeled PMU in bus #1 during a fault versus the idealized current phasor magnitude is given in Fig. 3. It can be seen that for this specific class-P PMU characterized by a window length of 3 periods and the timestamp centered in the window, the magnitude estimates take 4 time-steps to reach the pre-fault accuracy level. This aspect is taken into account in Section IV-D to assess the total latency of the proposed method.

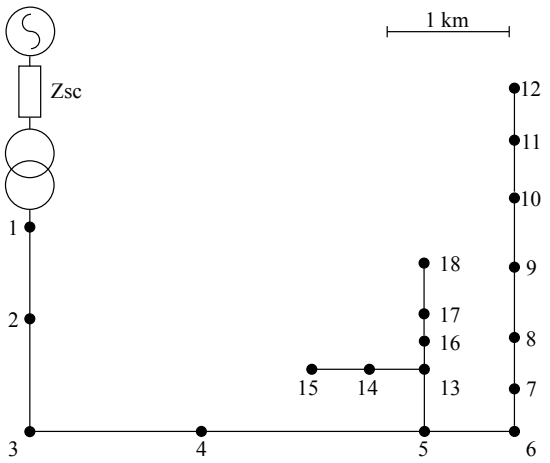

Fig. 2. The simulated 18-bus distribution feeder located in the Netherlands.

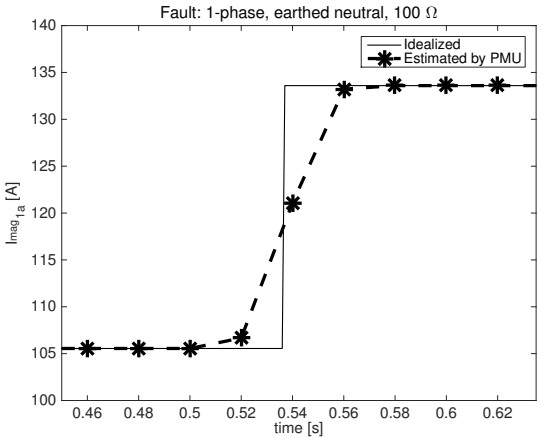

Fig. 3. Comparison between the current phasor magnitude estimated by the simulated PMU in bus #1 during a fault versus the idealized current phasor magnitude.

This article has been accepted for publication in a future issue of this journal, but has not been fully edited. Content may change prior to final publication. Citation information: DOI 10.1109/TPWRD.2016.2545923, IEEE Transactions on Power Delivery

C. Measurement noise model

In the literature, the robustness of fault detection and location algorithms is tested with respect to the measurement noise [12]. As mentioned in Section III-B, the simulated PMU introduces only the noise due to the synchrophasor estimation algorithm. It is then needed to superimpose a measurement noise to the synchrophasors estimated by the simulated PMU. The noise should also include the effect of the sensor interfacing the PMU to the network. In order to generate a realistic noise, real-field data have been used.

We have considered real measurements taken in the 20-kV distribution network of the Swiss federal institute of technology of Lausanne (EPFL), which has been equipped with PMUs at every bus measuring nodal voltage and injected current phasors. The whole infrastructure is described in [9]. The voltage sensors are 0.1-class capacity voltage dividers, while the current sensors are 0.5-class Rogowski coils [25]. They are connected to PMUs developed by the authors of this paper and described in [8], which are characterized by a sampling frequency of 10 kHz and a reporting rate of 50 frames-per-second. These real PMUs run the same synchrophasor estimation algorithm as the simulated ones used in this work.

Fig. 4 shows the magnitude and phase of nodal voltage and injected current measurements. Note that these measurements include the noise introduced by the combination of sensor and PMU. The corresponding standard deviations (stds) are:

$$\begin{aligned} \sigma_{V_{mag}} &= 1.6 \cdot 10^{-3}\% \quad \sigma_{V_{ph}} &&= 5.1 \cdot 10^{-5}[rad] \\ \sigma_{I_{mag}} &= 4.0 \cdot 10^{-1}\% \quad \sigma_{I_{ph}} &&= 5.8 \cdot 10^{-3}[rad] \end{aligned} \tag{19}$$

Furthermore, Fig. 5 shows that the Gaussian assumption of the measurement noises is fulfilled. The voltage and current phases are referred to the phase of another quantity (see Figs. 4b and 4d) because the phase is continuously changing due to the fact that the real system frequency is not exactly 50 Hz. The std of the voltage phase is $1/\sqrt{2}$ of the one of $(E_{ph_{1a}} - E_{ph_{5a}})$ since we assume that the two voltage noises have the same std and are uncorrelated (the same assumption holds for the voltage magnitude noise). On the contrary, we entirely attribute the noise of $(I_{ph_{1c}} - E_{ph_{1c}})$ to the current phase. It is important to observe that the graphs of Fig. 4 include both the measurement noise and the network dynamics, therefore the computed stds are overestimated.

Further assumptions have to be made in order to simulate the realistic behavior of the sensing system:

1) We use current protection sensors in bus #1 to measure the current during the fault. Their accuracy is assumed to be 10 times worse than the one defined in (19).
2) The 1-phase low impedance fault in an unearthed neutral network leads the voltage in the faulted phase to drop to around 0.6 % of the rated value. In this specific case, we consider an accuracy of these voltage measurements to be 100 times worse than the one defined in (19).

In Section IV we carry out a sensitivity analysis of the proposed fault location algorithm with respect to the measurement noise.

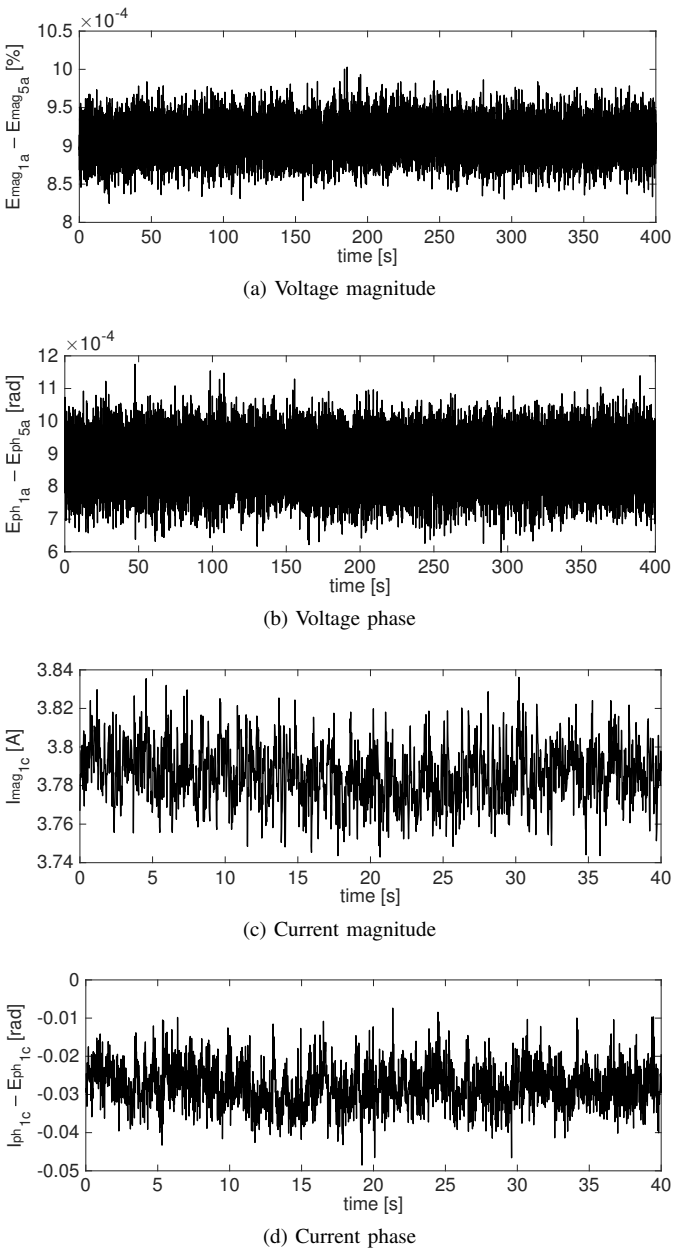

Fig. 4. Real voltage and current measurements taken in the 20-kV distribution network of the Swiss federal institute of technology of Lausanne (EPFL). These signals include the noise introduced by the combination of sensor and PMU. The noise stds inferred from these signals are shown in (19).

IV. Performance Assessment

The accuracy of the proposed method in identifying the line affected by the fault has been extensively tested. The scenarios refer to different combinations of the following factors:

- Low, high or very high impedance faults (1 Ω, 100 Ω or 1000 Ω);
- Symmetric (3-ph) or asymmetric (1-ph-to-ground and 2-ph) faults;
- Fault at 1/4 or 1/2 of the line length. Three lines are considered: $L_{4,5}$, $L_{9,10}$, $L_{13,16}$;
- Network operated with earthed or unearthed neutral;
- Presence of DG and different network operating conditions.

This article has been accepted for publication in a future issue of this journal, but has not been fully edited. Content may change prior to final publication. Citation information: DOI 10.1109/TPWRD.2016.2545923, IEEE Transactions on Power Delivery

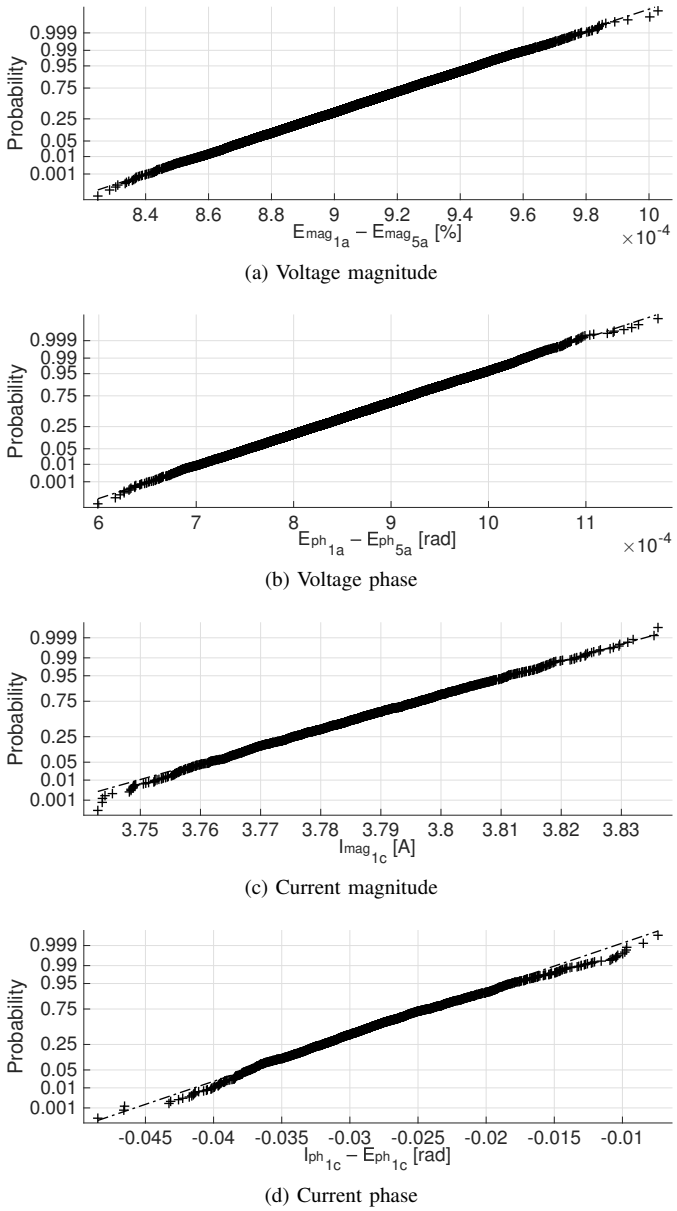

(a) Voltage magnitude

(b) Voltage phase

(c) Current magnitude

(d) Current phase

Fig. 5. Normal probability plots of the measured quantities shown in Fig. 4. The normality assumption of the measurement noises is satisfied.

A. Faulted line identification

For a given fault scenario (e.g., 1-ph-to-ground low impedance fault, at 1/4 of a specific line, on a network operated with earthed neutral, without DG), the procedure used to assess the accuracy of the proposed fault location method is the following:

1) The model is implemented and run in Simulink by using the Opal-RT RTS. The synchrophasors estimated by the PMUs at 50 frames-per-second are recorded.
2) M sets of measurements are obtained by perturbing the quantities inferred in step 1 with randomly-generated Gaussian white noise characterized by the stds given in Section III-C (M is equal to 10000 in order to get results that are statistically significant). Note that the phase noise std is in radians, while the magnitude noise std is in percentage of the quantity X of step 1. Therefore, the magnitude and phase of the synchrophasor measurement X_{meas} are calculated as follows:

$$\begin{aligned} X_{meas_{mag}} &= X_{mag} + N(0, \sigma_{X_{mag}} \cdot X_{mag}) \\ X_{meas_{ph}} &= X_{ph} + N(0, \sigma_{X_{ph}}) \end{aligned} \quad (20)$$

3) Each set of measurements computed in step 2 is given to the m parallel SEs that return the m estimated states. The latter are compared with the set of measurements in order to obtain m WMR values. The index of the SE exhibiting the lowest WMR identifies the inferred faulted line. The proposed fault location method is successful if the inferred faulted line coincides with the real faulted line.
4) The accuracy of the fault location method is represented by the percentage of success in correctly identifying the faulted line. It is computed as:

$$accuracy = \frac{M_s}{M} \cdot 100$$

where M_s indicates the number of times the faulted line is correctly identified and M represents the number of sets of noisy measurements generated for the specific fault. As already mentioned, we chose a high value of M (M=10000) in order to obtain statistically significant results.

The accuracy of the proposed fault location method for each scenario is given in Tables I-XI. The tables also contain an analysis of the sensitivity of the proposed fault location method accuracy with respect to the noise level (the noise level is directly linked to the accuracy of the sensors, as described in detail in the Appendix):

- *Noise level 1*: the noise stds are the ones presented in Section III-C, which are obtained from real 0.1-class voltage and 0.5-class current sensors;
- *Noise level 10*: the noise stds related to the *measurement* sensors and the current *protection* sensors in bus #1 are respectively 10 and 3 times larger than the ones presented in Section III-C. These values refer to significantly worse sensors and were chosen in order to represent a worst, but still realistic, scenario.

In order to provide an example, Fig. 6a shows the WMRs of the m-SEs as a function of time for the specific case of a 3-ph fault at a quarter of line $L_{13,16}$, with fault impedance of 100 Ω and *Noise level 1*. The fault occurs between 0.5 and 0.52 seconds. The quick separation of the WMRs in the following time-steps allows the detection of the fault according to the algorithm presented in Section II-B. After three time-steps (see Figs. 3 and 7), it is evident that the LWLS with the virtual bus in line $L_{13,16}$ maintains the lowest WMR, therefore the fault location algorithm correctly identifies the fault in line $L_{13,16}$. It is worth observing that the fault in line $L_{13,16}$ is the most challenging to be identified among the three considered lines. This is due to the fact that line $L_{13,16}$ and its neighbor lines ($L_{5,13}$, $L_{13,14}$ and $L_{16,17}$) are short (218 to 510 meters), and the virtual buses positioned in these lines are close to the fault. Indeed, we can see from Fig. 6a that the WMRs of the SEs using these virtual buses are quite close to each other. As a consequence, when we apply a high level of measurement

This article has been accepted for publication in a future issue of this journal, but has not been fully edited. Content may change prior to final publication. Citation information: DOI 10.1109/TPWRD.2016.2545923, IEEE Transactions on Power Delivery

noise, the WMRs become more noisy (see Fig. 6b), leading to a possible misestimation of the faulted line. However, it is important to point out that in the time-steps where the algorithm fails, it locates the fault in one of the lines adjacent to the faulted one.

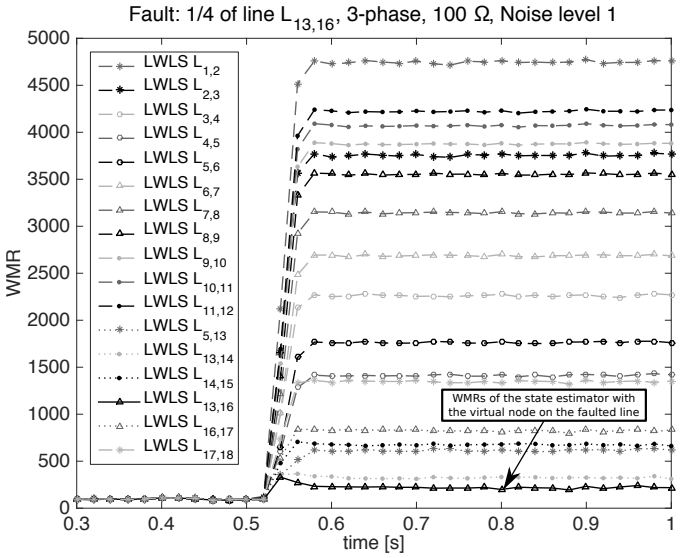

(a) Noise level 1.

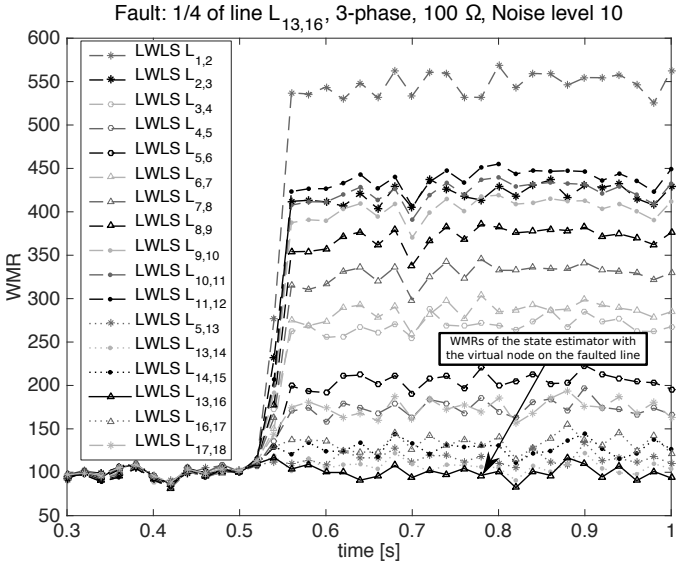

(b) Noise level 10.

Fig. 6. WMRs of the m-SEs in case of a 3-ph high impedance fault at a quarter of line $L_{13,16}$ occurring between 0.5 and 0.52 seconds. Two noise levels are shown: (a) *Noise level 1*; (b) *Noise level 10*. In (b) the noisy WMRs worsen the accuracy of the fault location method. At some time-steps, it does not locate the fault on the faulted line, but on one of the adjacent lines.

Tables I and II refer to symmetric faults, namely 3-ph. The low-impedance fault is characterized by a fault impedance of 1 Ω and leads to fault currents in the order of thousands of Amperes. The high-impedance fault is assumed to have a fault impedance of 100 Ω that produces a fault current limited to tens of Amperes. Consequently, the high-impedance faults are very difficult to identify and locate. Unlike conventional schemes, the proposed method guarantees a correct fault detection and location in case of realistic noise level (i.e. *Noise level 1*). If we increase the noise level (i.e. *Noise level 10*), the percentage of success decreases for the case of high impedance faults. Indeed, high impedance faults cause less perturbation in the network state compared to the low impedance ones. The WMRs of the various SEs are closer to each other and the method becomes more sensitive to the noise, as already explained above. However, even with the high noise level and the high fault impedance, the proposed method exhibits a quite high number of correct fault location estimates.

We can also notice that the algorithm is always less accurate in locating faults at a quarter of a line compared to the ones in the middle of a line. Indeed, the presented methodology assumes that each virtual bus is in the middle of a given line. However, in the experimental validation, the position of the fault was changed along the line (i.e. $\frac{1}{2}$ or $\frac{1}{4}$ of the line length) but always keeping the virtual bus of the SEs in the middle of the line. When the actual fault happens to be exactly in the virtual bus of one of the SEs (i.e. in the middle of the line), the network topology and the admittance matrix used by that SE match perfectly the simulated faulted network. For this reason, we achieve higher accuracy when the fault is in the middle of the line. However, we have shown that even for fault locations not on the virtual bus, we do achieve the correct identification of the faulted line.

The same considerations about symmetric faults can be extended to the other scenarios. We can further observe that the proposed fault location method has slightly reduced performance in locating a low impedance fault only in case of a 1-ph fault in an unearthed neutral network with *Noise level 10*. The reason is that the voltage drops significantly in the faulted phase. As already mentioned in Section III-C, for this specific case we have used stds of the voltage magnitude and phase measurements in the faulted phase which are 100 times larger than the ones defined in Section III-C.

As a conclusion, we can state that the proposed algorithm is able to correctly detect the fault and locate the faulted line irrespectively of the neutral connection, fault type, fault impedance and fault position. The method is robust against realistic noise levels since, during the experimental validation, it never failed when using noises directly inferred from real-field data. The fault location accuracy decreases, but not significantly, only when we apply a noise level 10 times larger. However, this noise level is considerably larger than the real one and the success percentage of proposed method remains above 66%.

In order to further test the proposed fault location method we have carried out another simulation with a higher fault impedance of 1 kΩ. This is commonly considered one of the highest possible fault impedances since it refers to the typical electrical resistance of a biological body. The performance of the proposed method has been assessed considering a 1 kΩ 1-ph-to-ground fault in an unearthed neutral network. The reason motivating this choice is that, for this case, the fault current is limited in amplitude by the high network zero-sequence impedance, so that its value becomes comparable to the currents absorbed by the loads. Indeed, the simulation results show that fault location is more difficult in unearthed networks. We consider the case of *Noise level 1* in order to

This article has been accepted for publication in a future issue of this journal, but has not been fully edited. Content may change prior to final publication. Citation information: DOI 10.1109/TPWRD.2016.2545923, IEEE Transactions on Power Delivery

TABLE I
3-PH FAULT, 1 Ω

Fault Position		Noise Level 1	Noise Level 10
$L_{4,5}$	1/4	100%	100%
	1/2	100%	100%
$L_{9,10}$	1/4	100%	100%
	1/2	100%	100%
$L_{13,16}$	1/4	100%	100%
	1/2	100%	100%

TABLE II
3-PH FAULT, 100 Ω

Fault Position		Noise Level 1	Noise Level 10
$L_{4,5}$	1/4	100%	99.27%
	1/2	100%	99.85%
$L_{9,10}$	1/4	100%	98.54%
	1/2	100%	99.90%
$L_{13,16}$	1/4	100%	84.65%
	1/2	100%	99.74%

TABLE III
2-PH FAULT: EARTHED NEUTRAL, 1 Ω

Fault Position		Noise Level 1	Noise Level 10
$L_{4,5}$	1/4	100%	100%
	1/2	100%	100%
$L_{9,10}$	1/4	100%	100%
	1/2	100%	100%
$L_{13,16}$	1/4	100%	100%
	1/2	100%	100%

TABLE IV
2-PH FAULT: EARTHED NEUTRAL, 100 Ω

Fault Position		Noise Level 1	Noise Level 10
$L_{4,5}$	1/4	100%	92.48%
	1/2	100%	92.91%
$L_{9,10}$	1/4	100%	89.56%
	1/2	100%	95.09%
$L_{13,16}$	1/4	100%	68.43%
	1/2	100%	91.73%

TABLE V
2-PH FAULT: UNEARTHED NEUTRAL, 1 Ω

Fault Position		Noise Level 1	Noise Level 10
$L_{4,5}$	1/4	100%	100%
	1/2	100%	100%
$L_{9,10}$	1/4	100%	100%
	1/2	100%	100%
$L_{13,16}$	1/4	100%	100%
	1/2	100%	100%

TABLE VI
2-PH FAULT: UNEARTHED NEUTRAL, 100 Ω

Fault Position		Noise Level 1	Noise Level 10
$L_{4,5}$	1/4	100%	92.41%
	1/2	100%	92.83%
$L_{9,10}$	1/4	100%	89.38%
	1/2	100%	95.20%
$L_{13,16}$	1/4	100%	67.57%
	1/2	100%	92.32%

TABLE VII
1-PH-TO-GROUND FAULT: EARTHED NEUTRAL, 1 Ω

Fault Position		Noise Level 1	Noise Level 10
$L_{4,5}$	1/4	100%	100%
	1/2	100%	100%
$L_{9,10}$	1/4	100%	100%
	1/2	100%	100%
$L_{13,16}$	1/4	100%	100%
	1/2	100%	100%

TABLE VIII
1-PH-TO-GROUND FAULT: EARTHED NEUTRAL, 100 Ω

Fault Position		Noise Level 1	Noise Level 10
$L_{4,5}$	1/4	100%	83.78%
	1/2	100%	99.99%
$L_{9,10}$	1/4	100%	95.05%
	1/2	100%	99.23%
$L_{13,16}$	1/4	100%	96.06%
	1/2	100%	99.36%

TABLE IX
1-PH-TO GROUND FAULT: UNEARTHED NEUTRAL, 1 Ω

Fault Position		Noise Level 1	Noise Level 10
$L_{4,5}$	1/4	100%	69.84%
	1/2	100%	87.28%
$L_{9,10}$	1/4	100%	72.69%
	1/2	100%	77.82%
$L_{13,16}$	1/4	100%	72.08%
	1/2	100%	79.33%

TABLE X
1-PH-TO GROUND FAULT: UNEARTHED NEUTRAL, 100 Ω

Fault Position		Noise Level 1	Noise Level 10
$L_{4,5}$	1/4	100%	70.95%
	1/2	100%	99.66%
$L_{9,10}$	1/4	100%	89.99%
	1/2	100%	97.94%
$L_{13,16}$	1/4	100%	87.56%
	1/2	100%	95.74%

TABLE XI
1-PH-TO GROUND FAULT: UNEARTHED NEUTRAL, 1000 Ω

Fault Position		Noise Level 1
$L_{4,5}$	1/4	80.94%
	1/2	99.99%
$L_{9,10}$	1/4	95.92%
	1/2	99.30%
$L_{13,16}$	1/4	95.93%
	1/2	99.32%

match the realistic noise measured in the real network. The results are provided in Table XI. It can be seen that, also for this extreme scenario, the proposed methodology is capable to identify the faulted line and type of fault in the large majority of the cases.

B. Faulted buses

The fault on a bus has not been discussed so far because we assume to have a PMU installed in every substation. Hence, the faulted bus and the fault type are easily detected by using the measurements of the PMU installed in the faulted bus. For example, in case of 1-ph fault in a bus of an unearthed neutral network: (i) the voltage zero-sequence component has a non-null value; (ii) the current magnitude in the faulted phase has a sudden jump of tens of Amperes.

C. Distributed generation

The performance of the method has been also assessed when dealing with faults in networks characterized by a large penetration of DG. The loads in bus #4, #10 and #17 have been coupled with variable pitch wind turbine models driving 160 kW squirrel cage asynchronous generators running at nominal speed. The power requested by the loads has been varied in order to create three different scenarios. *Case 1*: a passive network where the loads absorb approximately 1/4 of the rated power of the real secondary substation transformers and the DG does not cover the load demand. *Case 2*: an intermediate scenario where the loads absorb 50 % of the power of *Case 1*, but the network is still passive. *Case 3*: the loads absorb 10 % of the power of *Case 1* so that the DG

This article has been accepted for publication in a future issue of this journal, but has not been fully edited. Content may change prior to final publication. Citation information: DOI 10.1109/TPWRD.2016.2545923, IEEE Transactions on Power Delivery

TABLE XII
DISTRIBUTED GENERATION, UNEARTHED NEUTRAL: FAULT AT 1/4 OF $L_{13,16}$, 100 Ω

Scenario	Fault Type	Noise Level	
		1	10
Case 1	3-ph	100%	82.73%
	2-ph	100%	66.66%
	1-ph	100%	80.74%
Case 2	3-ph	100%	83.08%
	2-ph	100%	67.43%
	1-ph	100%	82.34%
Case 3	3-ph	100%	84.62%
	2-ph	100%	69.71%
	1-ph	100%	83.40%

production is abundantly larger than the load demand making the feeder exporting power towards the upstream grid. For these tests, we have used the case characterized by the worst accuracy performance, namely a high impedance fault (100 Ω) on line $L_{13,16}$ in an unearthed neutral network. Table XII shows the fault location accuracy for different fault types and noise levels. As expected, these results are close to the ones refferring to the same fault conditions shown in Tables II, VI and X. Indeed, the presence of DG does not change the performance of the proposed method since state estimation inherently not affected by the nature of the loads/generators.

D. Computation time and latency

The assessment of the speed of the algorithm in identifying the faulted line is a metric of interest when comparing the proposed method to existing fault location algorithms. In what follows we focus on two time latencies: (i) the computation time of the proposed method and (ii) the overall latency of the system to identify the faulted line.

The former is basically the time needed to compute the parallel SEs and then to go through the pseudo-algorithm shown in Fig. 1. The computation time is affected by many factors, such as the size of the network, the number of measurements, and the type of state estimation technique employed. The proposed method has been implemented in an Apple MacBook Pro with a 2.6 GHz CPU, 8 GB RAM, and MATLAB® 2014b. The SEs are implemented in series and the computation time to run all the m-SEs is 11.0 ms with a std of 0.8 ms.

The overall latency represents the time between the occurrence of the fault and its identification. It is worth noting that, in order to obtain a reliable and correct post-fault synchrophasor estimate, the PMUs have to process a dataset of raw-sampled waveforms that does not contain the instant in which the fault occurred. To clarify this aspect, Fig. 7 shows that whenever a fault occurs (e.g., in the grey area), three acquisition windows (W_1,W_2,W_3) are always corrupted. We remind that the adopted synchrophasor estimation algorithm [8] uses a window containing three periods of the fundamental frequency. Then, W_4 contains the post-fault waveform without any step

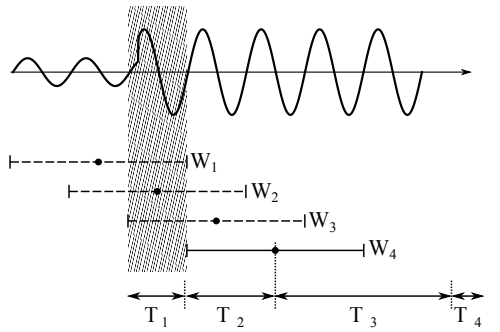

Fig. 7. Overall latency of the proposed method in identifying faults.

and the associated synchrophasor is correctly estimated. The total latency is therefore the sum of four contributions:

1) T_1 that is the time between the fault event and the first sample of window W_4. Depending on when the fault occurs in the grey area of Fig. 7, T_1 can vary between 0 and 20 ms;
2) T_2 that corresponds to half of the acquisition window length used by the synchrophasor estimation algorithm. Using the synchrophasor estimation algorithm described in [8], T_2 is equal to 30 ms at 50 Hz;
3) T_3 is the time between the center of the acquisition window and the moment the set of measurements is fed to the SEs. In [9], T_3 has been shown to be equal to 61 ms with a std of 1.8 ms;
4) T_4 is the computation time needed to run the m-SEs. For the case considered in this paper, T_4 is equal to 11 ms with a std of 0.8 ms.

Therefore, the overall latency can vary between 102 and 122 ms, depending on the instant the fault occurred.

V. CONCLUSIONS

This paper proposes a novel PMU-based fault detection and location method for ADNs using real-time state estimation. It consists in parallel SEs characterized by different and augmented network topologies in order to include a floating fault bus. By comparing the weighted measurement residuals of all the SEs, we are able to detect the presence of a fault and identify the faulted line with a latency ranging from 102 to 122 ms. The validation has been carried out by using a real 18-bus distribution network equipped with PMUs at every bus. The electrical network and the PMUs are simulated in the time-domain by using a RTS. We have also implemented the PMU synchrophasor estimation algorithm in order to reproduce the real PMU behavior. The measurement noises have been inferred from real-field PMU data. The proposed method correctly identifies the faulted line irrespectively of the neutral connection, fault type, fault impedance and fault position along the line. It has also been proven to be significantly robust against noise. Additionally, the fault location accuracy is not influenced by the presence of DG since the method is based on state estimation, which does not inherently depend on the nature of the loads/generators.

APPENDIX

This Appendix provides additional elements to replicate the results obtained in this work. In particular, Table XIII contains the zero and positive sequence electrical parameters of the lines composing the real distribution network adopted in this work and located in the Netherlands. Table XIV provides the stds adopted for the combination of *measurement* sensors and PMUs installed in all the buses but bus #1. The measurement stds corresponding to the case of *Noise level 1* and *Noise level 10* described in Section IV-A are given. Table XV provides the stds adopted for the combination of current *protection* sensors and PMUs assumed to be installed in bus #1. Current *protection* sensors are chosen because they have to be able to measure high fault currents.

REFERENCES

[1] "Protection of distribution systems with distributed energy resources," Joint Working Group B5/C6.26/CIRED, Tech. Rep., March 2015.

[2] J. Mora-Flòrez, J. Melèndez, and G. Carrillo-Caicedo, "Comparison of impedance based fault location methods for power distribution systems," *Electric Power Systems Research*, vol. 78, no. 4, pp. 657 – 666, 2008.

[3] A. Borghetti, M. Bosetti, C. Nucci, M. Paolone, and A. Abur, "Integrated use of time-frequency wavelet decompositions for fault location in distribution networks: Theory and experimental validation," *Power Delivery, IEEE Trans. on*, vol. 25, no. 4, pp. 3139–3146, Oct 2010.

[4] J. Ren, S. Venkata, and E. Sortomme, "An accurate synchrophasor based fault location method for emerging distribution systems," *Power Delivery, IEEE Transactions on*, vol. 29, no. 1, pp. 297–298, Feb 2014.

[5] D. Haughton and G. Heydt, "A linear state estimation formulation for smart distribution systems," *Power Systems, IEEE Transactions on*, vol. 28, no. 2, pp. 1187–1195, May 2013.

[6] J. Liu, J. Tang, F. Ponci, A. Monti, C. Muscas, and P. Pegoraro, "Trade-offs in PMU deployment for state estimation in active distribution grids," *Smart Grid, IEEE Transactions on*, vol. 3, no. 2, pp. 915–924, 2012.

[7] S. Sarri, L. Zanni, M. Popovic, J.-Y. Le Boudec, and M. Paolone, "Performance assessment of linear state estimators using synchrophasor measurements," *IEEE Transactions on Instrumentation and Measurement*, vol. 65, no. 3, pp. 535–548, March 2016.

[8] P. Romano and M. Paolone, "Enhanced interpolated-DFT for synchrophasor estimation in FPGAs: Theory, implementation, and validation of a PMU prototype," *Instrumentation and Measurement, IEEE Transactions on*, vol. 63, no. 12, pp. 2824–2836, Dec 2014.

[9] M. Pignati, M. Popovic, S. Barreto, R. Cherkaoui, G. Dario Flores, J.-Y. Le Boudec, M. Mohiuddin, M. Paolone, P. Romano, S. Sarri, T. Tesfay, D.-C. Tomozei, and L. Zanni, "Real-time state estimation of the EPFL-campus medium-voltage grid by using PMUs," in *Innovative Smart Grid Technologies Conference (ISGT), 2015 IEEE Power Energy Society*, Feb 2015, pp. 1–5.

[10] A. von Meier, D. Culler, A. McEachern, and R. Arghandeh, "Micro-synchrophasors for distribution systems," in *Innovative Smart Grid Technologies Conference (ISGT), 2014 IEEE PES*, Feb 2014, pp. 1–5.

[11] M. Shiroei, S. Daniar, and M. Akhbari, "A new algorithm for fault location on transmission lines," in *Power Energy Society General Meeting, 2009. PES '09. IEEE*, July 2009, pp. 1–5.

[12] P. Janssen, "Monitoring, protection and fault location in power distribution networks using system-wide measurements," Ph.D. dissertation, Ecole Polytechnique de Bruxelles, 2013-2014.

[13] A. Abur and A. Exposito, *Power system state estimation: theory and implementation*. CRC, 2004, vol. 24.

[14] P. Navalkar and S. Soman, "Secure remote backup protection of transmission lines using synchrophasors," *Power Delivery, IEEE Transactions on*, vol. 26, no. 1, pp. 87–96, Jan 2011.

[15] A. Abur, H. Kim, and M. Celik, "Identifying the unknown circuit breaker statuses in power networks," *Power Systems, IEEE Transactions on*, vol. 10, no. 4, pp. 2029–2037, Nov 1995.

[16] F. Wu and W.-H. Liu, "Detection of topology errors by state estimation [power systems]," *Power Systems, IEEE Transactions on*, vol. 4, no. 1, pp. 176–183, Feb 1989.

[17] E. Andreoli, A. Costa, and K. Clements, "Topology validation via simultaneous state & topology estimation with phasor data processing capability," in *Power Systems Computation Conference (PSCC), 2014*, Aug 2014, pp. 1–7.

[18] V. Freitas and A. Simoes Costa, "Integrated state & topology estimation based on a priori topology information," in *PowerTech, 2015 IEEE Eindhoven*, June 2015, pp. 1–6.

[19] E. Caro, R. Singh, B. Pal, A. J. Conejo, and R. Jabr, "Participation factor approach for phasor measurement unit placement in power system state estimation," *IET generation, transmission & distribution*, vol. 6, no. 9, pp. 922–929, 2012.

[20] J. Zhang, G. Welch, G. Bishop, and Z. Huang, "A two-stage kalman filtering approach for robust and real-time power systems state tracking," *IEEE Trans. Sustain. Energy*, vol. 5, no. 2, p. 629636, 2014.

[21] Microgrid at Illinois Institute of Technology. [Online]. Available: http://www.iitmicrogrid.net/

[22] M. Pignati, L. Zanni, S. Sarri, R. Cherkaoui, J.-Y. Le Boudec, and M. Paolone, "A pre-estimation filtering process of bad data for linear power systems state estimators using PMUs," in *Power Systems Computation Conference (PSCC), 2014*, Aug 2014, pp. 1–8.

[23] Cyber-secure data and control cloud for power grids. [Online]. Available: http://www.cdax.eu/

[24] P. Romano, M. Pignati, and M. Paolone, "Integration of an IEEE std. c37.118 compliant PMU into a real-time simulator," in *the 2015 IEEE PowerTech Conference*, 2015.

[25] Altea solutions. [Online]. Available: http://www.alteasolutions.eu/

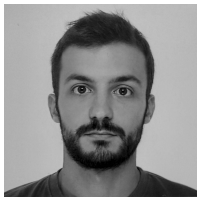

Marco Pignati (M'13) received the B.Sc. and M.Sc. degrees (Hons.) in electrical engineering from the University of Bologna, Italy, in 2009 and 2012, respectively. He is currently pursuing the Ph.D. degree with the Distributed Electrical System Laboratory, Swiss Federal Institute of Technology of Lausanne, Switzerland. His current research interests include real-time monitoring and control of active distribution networks with particular focus on synchrophasor-based applications.

Lorenzo Zanni (M'13) was born in Italy in 1988. He received the B.Sc. and M.Sc. (Hons.) degrees in electrical engineering from the University of Bologna, Bologna, Italy, in 2010 and 2012, respectively. He is currently pursuing the Ph.D. degree with the Distributed Electrical System Laboratory, École Polytechnique Fédérale de Lausanne, Lausanne, Switzerland. His current research interests include real-time monitoring and control of active distribution networks with particular focus on state estimation using phasor measurement units, and synchrophasor-based fault location.

Paolo Romano (M'12) is a Postdoctoral fellow at the Distributed Electrical Systems Laboratory (DESL) of the Swiss Federal Institute of Technology of Lausanne (EPFL). He received his BSc and MSc degree (with honors) in electronics engineering from the University of Genova, Italy, in 2008 and 2011 respectively, and his Ph.D. from the Swiss Federal Institute of Technology of Lausanne in 2016. His research interests refer to the synchrophasor area and particularly to the development of advanced Phasor Measurement Units for the real-time monitoring of active distribution networks.

This article has been accepted for publication in a future issue of this journal, but has not been fully edited. Content may change prior to final publication. Citation information: DOI 10.1109/TPWRD.2016.2545923, IEEE Transactions on Power Delivery

TABLE XIII
ELECTRICAL PARAMETERS OF THE LINES

	length $[km]$	R_0 $[\frac{\Omega}{km}]$	X_0 $[\frac{\Omega}{km}]$	B_0 $[\frac{S}{km}]$	R_P $[\frac{\Omega}{km}]$	X_P $[\frac{\Omega}{km}]$	B_P $[\frac{S}{km}]$
$L_{1,2}$	0.74464	1.0571	0.9104	7.3390e-5	0.1393	0.0752	1.4794e-4
$L_{2,3}$	0.92883	1.0568	0.9095	7.6043e-5	0.1393	0.0752	1.4718e-4
$L_{3,4}$	1.43843	0.8439	0.1967	1.1959e-5	0.1593	0.0874	1.4495e-4
$L_{4,5}$	1.81345	1.0405	0.8551	7.1209e-5	0.1408	0.0761	1.4942e-4
$L_{5,6}$	0.7059	0.8150	0.1000	1.4137e-5	0.1620	0.0890	1.4137e-4
$L_{6,7}$	0.31992	0.8150	0.1000	1.4137e-5	0.1620	0.0890	1.4137e-4
$L_{7,8}$	0.4312	0.8150	0.1000	1.4137e-5	0.1620	0.0890	1.4137e-4
$L_{8,9}$	0.5916	0.8150	0.1000	1.4137e-5	0.1620	0.0890	1.4137e-4
$L_{9,10}$	0.56363	0.8150	0.1000	1.4137e-5	0.1620	0.0890	1.4137e-4
$L_{10,11}$	0.45427	0.8150	0.1000	1.4137e-5	0.1620	0.0890	1.4137e-4
$L_{11,12}$	0.42235	1.2369	1.3535	5.5964e-5	0.3571	0.0824	1.0621e-4
$L_{5,13}$	0.51052	1.0600	0.9200	7.3828e-5	0.1390	0.0750	1.4765e-4
$L_{13,14}$	0.457	1.0600	0.9200	7.3828e-5	0.1390	0.0750	1.4765e-4
$L_{14,15}$	0.47166	1.0600	0.9200	7.3828e-5	0.1390	0.0750	1.4765e-4
$L_{13,16}$	0.22738	1.2400	1.3800	5.3407e-5	0.3560	0.0820	1.0681e-4
$L_{16,17}$	0.21808	1.2400	1.3800	5.3407e-5	0.3560	0.0820	1.0681e-4
$L_{17,18}$	0.41697	1.1922	0.9745	8.7439e-5	0.3734	0.0883	1.0003e-4

TABLE XIV
MEASUREMENT SENSORS AND PMU ACCURACY

Noise level 1	$\sigma_{V_{mag}} = 1.6 \cdot 10^{-3}$ %	$\sigma_{V_{ph}} = 5.1 \cdot 10^{-5}$ [rad]
	$\sigma_{I_{mag}} = 4.0 \cdot 10^{-1}$ %	$\sigma_{I_{ph}} = 5.8 \cdot 10^{-3}$ [rad]
Noise level 10	$\sigma_{V_{mag}} = 1.6 \cdot 10^{-2}$ %	$\sigma_{V_{ph}} = 5.1 \cdot 10^{-4}$ [rad]
	$\sigma_{I_{mag}} = 4.0$ %	$\sigma_{I_{ph}} = 5.8 \cdot 10^{-2}$ [rad]

TABLE XV
CURRENT PROTECTION SENSORS AND PMU ACCURACY

Noise level 1	$\sigma_{I_{mag}} = 4.0$ %	$\sigma_{I_{ph}} = 5.8 \cdot 10^{-2}$ [rad]
Noise level 10	$\sigma_{I_{mag}} = 12.0$ %	$\sigma_{I_{ph}} = 1.7 \cdot 10^{-1}$ [rad]

Rachid Cherkaoui (M'05-SM'07) received both the M.Sc. and Ph.D. degrees in electrical engineering in 1983 and 1992, respectively, from the Swiss Federal Institute of Technology in Lausanne (EPFL), Switzerland. He is currently Senior scientist at EPFL, leading the power systems group. His research interests are in electricity market deregulation, distributed generation and storage, and power system vulnerability mitigation.

He is member of technical program committees of various conferences and was member of CIGRE TF's and WG's. He was IEEE Swiss chapter officer from 2005 to 2011. He is author and co-author of more than 100 scientific publications.

Mario Paolone (SM'10) received the M.Sc. (Hons.) and Ph.D. degrees in electrical engineering from the University of Bologna, Bologna, Italy, in 1998 and 2002, respectively.

He was appointed as an Assistant Professor of Power Systems with the University of Bologna in 2005, where he was with the Power Systems Laboratory until 2011. He is currently an Associate Professor with the École Polytechnique Fédérale de Lausanne, Switzerland, where he was the EOS Holding Chair of the Distributed Electrical Systems Laboratory. He has authored or co-authored over 200 scientific papers in reviewed journals and international conferences. His current research interests include power systems with particular reference to real-time monitoring and operation, power system protections, power systems dynamics, and power system transients.

Dr. Paolone received the Associate Professor eligibility from the Politecnico di Milano, Milan, Italy, in 2010. In 2013, he was a recipient of the IEEE Electromagnetic Compatibility Society Technical Achievement Award. He was the Co-Chair of the Technical Program Committees of the Ninth Edition of the International Conference of Power Systems Transients in 2009 and the Power Systems Computation Conference in 2016. He is the Editor-in-Chief of the Sustainable Energy, Grids and Networks (Elsevier) journal.